Dispersion relations for plasmons in complex-shaped nanoparticle chains

Anton M. Pikalov,[1] Alexander V. Dorofeenko,[2,3,4,*] and Yurii E. Lozovik[3,5,6]

[1]*Physics Department, M.V. Lomonosov Moscow State University, 1 Leninskie Gory, Moscow 119991, Russia*

[2]*Institute for Theoretical and Applied Electromagnetics, 13 Izhorskaya, Moscow 125412, Russia*

[3]*Dukhov Research Institute of Automatics, 22 Suschevskaya, Moscow 127055, Russia*

[4]*Moscow Institute of Physics and Technology, 9 Institutskiy pereulok, Dolgoprudny 141700, Moscow Region, Russia*

[5]*Institute for Spectroscopy RAS, 5 Fizicheskaya, Troitsk 142190, Russia*

[6]*National Research University Higher School of Economics, 20 Myasnitskaya, Moscow 101000, Russia*

(Received 11 June 2018; published 21 August 2018)

A method for finding dispersion in chains of plasmonic particles of arbitrary shape is proposed. Our approach is based on analytic continuation via polylogarithms and is basically a generalization of the method known for spherical nanoparticle chains. As an example, we consider an axial chain of split-ring resonators. Three distinct solutions are distinguished, namely, two plasmons and a nonexponential wave. Dispersion relations, decay profiles, and spectra of excitation by a point source are obtained and compared with that in a spherical nanoparticle chain. The nuances of implementing the method are discussed.

DOI: 10.1103/PhysRevB.98.085134

I. INTRODUCTION

Plasmonic chains have been of great interest since it was discovered that a chain consisting of spherical metal nanoparticles can possess guiding properties due to electromagnetic coupling [1]. Owing to their plasmonic nature, such waveguides provide high oscillation frequency (up to $\sim$1000 THz) and strong confinement of electromagnetic field. This opens up opportunities for creating optoelectronic devices for operating with optical signals at nanoscale.

The central issue of theoretical investigations of plasmonic chain waveguides is determining their dispersion properties. Although it is a common knowledge when it concerns longitudinally homogeneous plasmonic waveguides like metallic nanowires [2], this problem turned out to be unexpectedly difficult with particle chains. The confusion occurs when one tries to consider a general case of infinite particle chain taking into account inter-particle interactions at arbitrarily long distances. The local field acting on a certain particle from all other particles is represented by a series that diverges that leads to an unsolvable dispersion equation [3,4].

For this reason, many approximate methods for determining dispersion relations in plasmonic chain waveguides were developed to avoid the infinite summation problem. The simplest one is based on the nearest-neighbor approximation (NNA). It was used to find dispersion in chain of spherical nanoparticles in quasistatic limit [5]. It was also applied to a split-ring resonator (SRR) waveguide [6].

Another approach is connected with consideration of finite chains, which gives a possibility to take into account all interactions between the particles. Then the dispersion properties can be retrieved from the oscillation patterns in the finite chain. Maier *et al.* [7] uses numerical FDTD simulation of excitation of a finite chain of nanospheres by a point dipole oscillating at different frequencies. Then the excited waves are analyzed to determine the values of wave number and attenuation factor. A similar method using spatial Fourier transform was employed to find dispersion in chain of SRRs. Both numerical and experimental data were used [8].

Another retrieval technique was proposed by Weber and Ford [9]. They search for eigenfrequencies of a finite chain of spherical nanoparticles. The corresponding eigenmodes take a form of standing waves that gives the values of wavelength and corresponding wave numbers. Each pair of eigenfrequency and wave number gives a point at the dispersion diagram (N points total for a N-particle chain). Thus, the method selects a discrete set of points from a continuous dispersion curve (as a finite chain selects a discrete set of modes from the whole spectrum). The drawback of the method is that increasing density of points is a computationally expensive problem since it requires solving the $2N$th power equation for a N-particle chain.

Attempts to take into account all interparticle interactions in an infinite chain lead to a dispersion equation containing an infinite sum that diverges at complex k or complex ω [3,4]. Yet, it can be calculated assuming both k and ω real. One can plot a map of the absorption rate in the coordinates of real values of k and ω with fuzzy "dispersion-like" regions where relationship of k and ω comes close enough to a true dispersion relation. This approach to approximate the dispersion curves was used in Refs. [10,11]. Its obvious disadvantage is difficulties to deal with highly damped waves (when complex k and ω that belong to a true dispersion have large imaginary parts) and inability to gauge numerically waves attenuation.

An exact method of finding dispersion in chains of spherical nanoparticles was developed by Koenderink [4] (see also Ref. [12]). It involves analytical summation of the infinite sums in the domain of convergence and analytical continuation to the domain of all complex values of k and ω. This makes possible to find exact complex-valued solution of the dispersion equation

*adorofeenko@itae.ru

Since there is an ambiguity in the choice of k and ω, there are two cases that are generally used, ω complex at k real and k complex at ω real [13]. These two cases correspond to physically different problems, to pulse excitation of the chain by a plane wave and to stationary excitation by a point source, respectively. Thus, the first case is more preferable for description of lumped systems with dumping, while the second one for distant propagation.

Another method based on analytical continuation was proposed by Capolino [14]. It involves Ewald summation technique and allows us to classify solutions by guidance or radiance, proper or improper, etc.

Along with chains of nanospheres, other particles shapes are studied, e.g., cubes [15], rods [16], split-rings [17], holes [18,19], sandwiches [20], etc. However, exact dispersion relations cannot be found in such systems using existing methods as they rely strongly on point dipole approximation that is satisfactory for spherical nanoparticles but is not applicable for more complex shapes. Direct adaptation of the aforementioned methods is not possible in this case.

We propose the method of finding dispersion in chains of plasmonic nanoparticles of complex shapes. Specifically, we demonstrate it by example of an axial chain of split-ring resonators (such waveguides were already extensively studied in the microwave region [6,21]). Our approach is basically a generalization of the method developed for spherical nanoparticle chains by Koenderink [4]. The comprehensive analysis is given for both cases of spherical and complex-shaped nanoparticles waveguides. We work in the complex k representation, meaning studying distant plasmon propagation from a stationary source.

II. PROBLEM OF FIELD SUMMATION IN INFINITE CHAINS

Consideration of all pairwise particle interactions in infinite chain results in the equations including infinite number of interparticle interaction terms in the form $S = \sum_{n=1}^{\infty} s_n$. There are two possible approaches allowing to take into account all s_n terms, namely, sequential and simultaneous (analytical) summation.

In frame of the first approach one performs a sequent term-by-term summation of some large number N of the s_n terms, taking each of them individually. It may intuitively seem that the increase of N makes the sum to asymptotically tend to its true value S, $\sum_{n=1}^{N} s_n \underset{N\to\infty}{\to} S$. In this case, any arbitrary accuracy of the solution can be provided by adding enough number of terms. However, we show that this actually doesn't happen (see Supplemental Material [22]), namely, the increase of finite number of terms does not lead to the correct solution.

The second approach suggests that all the s_n terms can be taken into account *simultaneously* by an analytic summation. This approach requires that one managed to find an analytic sum of the series $S = \sum_{n=1}^{\infty} s_n$, which in turn requires that all inter-particle interaction terms are described by a unified analytical expression. An example of a system where this expression is known is a chain of point dipoles, which is a common model for spherical nanoparticle chains. The analytical approach to such chains is developed in Ref. [4] (see also Ref. [23]).

However, there is no expression of this kind for the vast majority of complex-shaped nanoparticles that means that their interaction can be calculated only numerically for any finite n. In this paper, we solve the problem of finding the dispersion relation of the complex-shaped nanoparticle chain by a semi-analytical approach, in which we start with a numerical calculation of interparticle interaction in a finite number of points. With the use of them, we then search an analytical function that represents the interparticle interaction at any (both small and infinitely large) distances and then apply the analytical summation approach.

III. WAVES IN CHAINS OF SPHERICAL NANOPARTICLES

Analysis of the arbitrarily-shaped particle chains will be largely based on the theory of spherical nanoparticle chains, which is known from Refs. [4,12,23]. Therefore, let us first consider a chain of spherical nanoparticles excited by an external electrical field of a frequency ω, inhomogeneously distributed along the chain and directed perpendicularly to the chain axis (transverse polarization, see Fig. 1). This field can be produced by an incident wave or a near-field source. Let us find a distribution of dipole moments excited by this field.

We follow a single dipole approximation (SDA), in which each particle is treated as a point dipole described by a sole dipole moment p_n. The latter appears as a response of the particle to an external field E^{ext} and to the field produced by interaction with other particles:

$$p_n = \alpha^{(s)} \sum_{m\neq n} g_{nm}^{(s)} p_m + \alpha^{(s)} E_n^{\text{ext}}. \tag{1}$$

Here $\alpha^{(s)}$ is a particle polarizability and $g_{nm}^{(s)}$ is a function that characterizes particle interaction. Because of translational invariance, it depends only on the difference between n and m, but not on each of them separately. Thus, further in the text a notation $g_m^{(s)}$ with one subscript is used, which means interaction of two particles at distance of m periods. The superscript "(s)" standing for "spherical" refers to all quantities related to spherical particles.

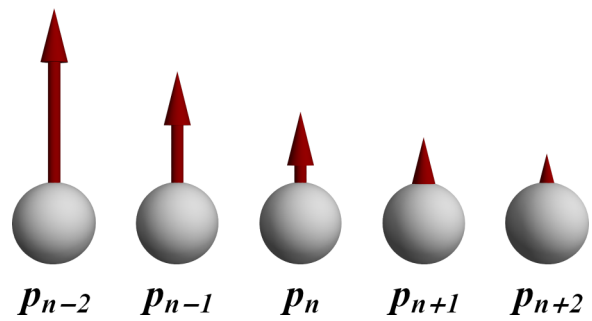

FIG. 1. Chain of spherical metallic particles. In exponentially decaying wave, the sum of the local fields created at any given particle diverges due to the exponential divergence of dipole amplitude in the negative direction.

In the case of SDA, $g_m^{(s)}$ takes the form of a field of a unitary dipole with respect to the transverse polarization,

$$g_m^{(s)} = \frac{1}{4\pi\varepsilon_0}\left(-\frac{1}{|md|^3} + \frac{ik_0}{|md|^2} + \frac{k_0^2}{|md|}\right) \times \exp(ik_0 d|m|), \quad m \neq 0, \tag{2}$$

where d is a chain period and $k_0 = \omega/c$ is a free-space wave number.

Polarizability of a spherical particle can be found as [9,24, Sec. 8.2.1 in 25,26]

$$\frac{1}{\alpha^{(s)}} = \frac{1}{4\pi\varepsilon_0}\left(\frac{\varepsilon+2}{\varepsilon-1}\frac{1}{a^3} - i\frac{2}{3}k_0^3\right), \tag{3}$$

where ε is a permittivity of the particle material (in our case, silver) and a is the particle radius. For a frequency dependence of ε we use the experimental data obtained by Babar [27] for silver. The frequency of dipole resonance of a single spherical particle (corresponding to $\varepsilon = -2$) is thereby $\omega_0^{(s)} = 5.36 \times 10^{15}\mathrm{s}^{-1}$. The frequency of the quadrupole resonance, which restricts the applicability of single-dipole approximation, which corresponds to $\varepsilon = -3/2$, is $\omega_1^{(s)} = 5.5 \times 10^{15}\mathrm{s}^{-1}$.

Now we involve Fourier representation introducing notations for Fourier transform of the dipole moments and external field distributions:

$$p(k) = (2\pi)^{-1}\sum_n p_n \exp(-iknd), \tag{4}$$

$$e(k) = (2\pi)^{-1}\sum_n E_n^{\mathrm{ext}} \exp(-iknd), \tag{5}$$

assuming at this stage that wave number k is real. Then, taking the Fourier transform of both parts of Eq. (1), we obtain[1]

$$p(k) = \alpha^{(s)}\Sigma_0^{(s)}(k)p(k) + \alpha^{(s)}e(k). \tag{6}$$

Here, a spectral function of real argument k is introduced:

$$\Sigma_0^{(s)}(k) = \sum_{m\neq 0} g_m^{(s)} e^{ikmd}. \tag{7}$$

Thus, the solution of the problem in the Fourier representation takes the form

$$p(k) = \frac{\alpha^{(s)}e(k)}{1 - \alpha^{(s)}\Sigma_0^{(s)}(k)}. \tag{8}$$

Return to the real space is made by the inverse Fourier transform,

$$p_n = \int_{-\pi}^{\pi} \frac{\alpha^{(s)}e(k)\exp(ikn)}{1 - \alpha^{(s)}\Sigma_0^{(s)}(k)}dk. \tag{9}$$

[1]In fact, series in Eq. (9) show mere conditional convergence due to the term $\sum_{m\neq 0} e^{ik_0 dm}/|m|$. This makes the derivation of Eq. (6) through a Fourier transform of Eq. (1), strictly speaking, incorrect, as well as the further analytic continuation. This fact has not been noticed in a number of papers dedicated to study of plasmons in infinite chains [3,4,12,28]. Despite this, a more rigorous derivation with an emphasis on convergence of series shows that Eq. (6) is correct and outcomes of said papers remain valid. See Ref. [23] for details.

Equation (9) allows us to find distribution of dipole moments p_n generated by an arbitrary source via its Fourier transform $e(k)$.

Note that only the real wave numbers k were considered so far. To deal with surface plasmons, we should take the complex values of k into consideration. To do this, we rewrite the function $\Sigma_0^{(s)}(k)$ with separating the series Eq. (7) into two subseries with positive and negative m,

$$\Sigma_0^{(s)}(k) = \frac{1}{4\pi\varepsilon_0}\frac{1}{d^3}\sum_{m=1}^{+\infty}\left(-\frac{1}{m^3} + \frac{ik_0 d}{m^2} + \frac{(k_0 d)^2}{m}\right)e^{i(k_0+k)md} + \frac{1}{4\pi\varepsilon_0}\frac{1}{d^3}\sum_{m=1}^{+\infty}\left(-\frac{1}{m^3} + \frac{ik_0 d}{m^2} + \frac{(k_0 d)^2}{m}\right)e^{i(k_0-k)md}. \tag{10}$$

Considering k complex, one can see that first and second series in Eq. (10) diverge at lower and upper complex half-plane, respectively. Thereby, function $\Sigma_0^{(s)}(k)$ can be defined only at the real axis $\mathrm{Im}(k) = 0$. To extend the application of Eq. (9) to all complex wave numbers, one must find analytic continuation of the function $\Sigma_0^{(s)}(k)$ to the entire complex plane.[1] In our case, it can be done by using polylogarithms $\mathrm{Li}_s(x) = \sum_{m=1}^{\infty} x^m/m^s$ [3,29]:

$$\Sigma^{(s)}(k) = -\frac{1}{4\pi\varepsilon_0}\frac{1}{d^3}[\mathrm{Li}_3(e^{i(k_0+k)d}) + \mathrm{Li}_3(e^{i(k_0-k)d})] + \frac{ik_0 d}{4\pi\varepsilon_0}\frac{1}{d^3}[\mathrm{Li}_2(e^{i(k_0+k)d}) + \mathrm{Li}_2(e^{i(k_0-k)d})] + \frac{(k_0 d)^2}{4\pi\varepsilon_0}\frac{1}{d^3}[\mathrm{Li}_1(e^{i(k_0+k)d}) + \mathrm{Li}_1(e^{i(k_0-k)d})]. \tag{11}$$

Polylogarithms in Eq. (11) can be calculated with an arbitrary precision for any complex k. This feature is added to many mathematical software such as Wolfram Mathematica, MatLab, Maple. Thus, the function $\Sigma^{(s)}(k)$ is an analytic continuation of the function $\Sigma_0^{(s)}(k)$, and one can obtain the distribution of dipole moments as

$$p_n = \int_{\mathbb{R}} \frac{\alpha^{(s)}e(k)\exp(ikn)}{1 - \alpha^{(s)}\Sigma^{(s)}(k)}dk. \tag{12}$$

Note that integration is carried out along the real axis, which is reduced to the integration over the range $[-\pi, \pi]$ because of the discreteness of nanoparticle chain.

Now let us consider a chain excited by a single δ-source, i.e., assume that a unitary external field acts only on the mth particle (in this case the required dipole moments distribution is the Green function),

$$E_n^{\mathrm{ext}} = \delta_{nm}. \tag{13}$$

Fourier transform of this source is

$$e(k) = (2\pi)^{-1} e^{-ikmd}. \tag{14}$$

Using this, we find dipole moments distribution according to Eq. (9),

$$p_n = \frac{1}{2\pi} \int_{\mathbb{R}} \frac{\alpha^{(s)} \exp\left(ik(n-m)\right)}{1 - \alpha^{(s)} \Sigma^{(s)}(k)} dk. \tag{15}$$

Integration in Eq. (15) is represented at the complex plane as contour integration along the real axis. Path of the integration can be deformed in any way unless it crosses singularities of the integrand. Considering separately the cases of $n - m \geqslant 0$ and $n - m \leqslant 0$, which physically mean consideration of particles located to the right and to the left of the δ-source, respectively, one can notice that the integrand tends to zero at $\mathrm{Im}k \to +\infty$ in the first case and at $\mathrm{Im}k \to -\infty$ in the second case. Thus, one can shift the path of integration to the upper complex half-plane in the case of $n - m \geqslant 0$ and to the lower half-plane in the case of $n - m \leqslant 0$. In the course of such path deformation, the integral in Eq. (15) breaks into several parts taken around every singularity of the integrand (see Fig. 2).

The singularities of the integrand in Eq. (15) are the two poles and one brunch cut.[2] Thus, total dipole moments distribution in a spherical nanoparticle chain contains three contributions,

$$p_n = p_{n,\mathrm{pole}\,1} + p_{n,\mathrm{pole}\,2} + p_{n,\mathrm{cut}}. \tag{16}$$

Integrals taken around the poles can be transformed using the residue theorem,

$$\begin{aligned} p_{n,\mathrm{pole}} &= \frac{1}{2\pi} \oint_{\mathrm{pole}} \frac{\alpha^{(s)} \exp\left(ik(n-m)\right)}{1 - \alpha^{(s)} \Sigma^{(s)}(k)} dk \\ &= i\,\mathrm{Res}_{\mathrm{pole}} \left[\frac{\alpha^{(s)} \exp\left(ik(n-m)\right)}{1 - \alpha^{(s)} \Sigma^{(s)}(k)} \right] \\ &= i \frac{\alpha^{(s)} \exp(ik_{\mathrm{pole}}(n-m))}{-\alpha^{(s)} \Sigma^{(s)\prime}(k_{\mathrm{pole}})}. \end{aligned} \tag{17}$$

Therefore, all the pole contributions $p_{n,\mathrm{pole}}$ take a form of exponentially decaying harmonic waves (plasmons) with the complex wave numbers k_{pole}. These wave numbers can be found from the condition of equality of denominator in (15) to zero,

$$1 - \alpha^{(s)} \Sigma^{(s)}(k) = 0, \tag{18}$$

where $\alpha^{(s)}$ and $\Sigma^{(s)}(k)$ are given by Eqs. (3) and (11), respectively.

This is a dispersion equation of plasmons in a chain of spherical nanoparticles. It also can be obtained directly from Eq. (1) setting external field to zero and substituting

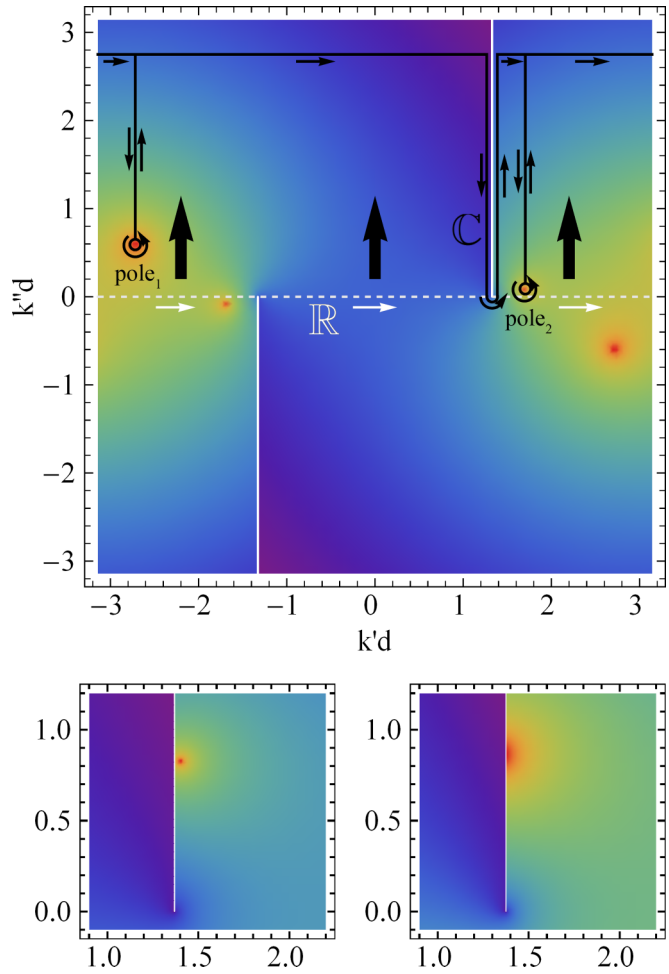

FIG. 2. A schematic (the losses are artificially reduced for the sake of visibility) plot of an absolute value of the integrand $1/(1 - \alpha\Sigma(k' + ik''))$ in Eq. (15) at the complex k plane (shown in color). The horizontal white dashed line is the original integration path, black solid line is the path after the shift. Thick arrows show the direction of shift. Thin arrows show the direction of integration. On the bottom, a pole hiding under the branch cut is shown on a larger scale.

infinite series with polylogarithms as it was done in a number of previous studies [3,4,28]. Such approach, though, allows only obtain wave numbers of plasmonic solutions, whereas the approach developed here gives also plasmon amplitudes excited by a source and additional nonexponential solution, which appears beside the plasmonic ones.

Contribution $p_{n,\mathrm{cut}}$ related to integration around the branch cut,

$$p_n = \frac{1}{2\pi} \int_{\mathbb{C}} \frac{\alpha^{(s)} \exp\left(ik(n-m)\right)}{1 - \alpha^{(s)} \Sigma^{(s)}(k)} dk \tag{19}$$

has a nonexponential decay profile as it includes a continuum of complex harmonics concentrated around a free space wave number. Waves of this type in plasmonic chains were first distinguished by Fung [28] although decay profiles of a nonexponential nature can be clearly observed in earlier works [1,9,30]. An important feature of a nonexponential contribution is that it always decays slower at long distances than any of

[2]The total number of poles in a particular region of the complex plane can be counted using the argument principle, taking into account that the integrand in Eq. (15) does not go anywhere to zero. In the present study poles are searched in a rectangular region $[-\pi, \pi]$ along real axis and $[0, 16\pi]$ along the imaginary axis.

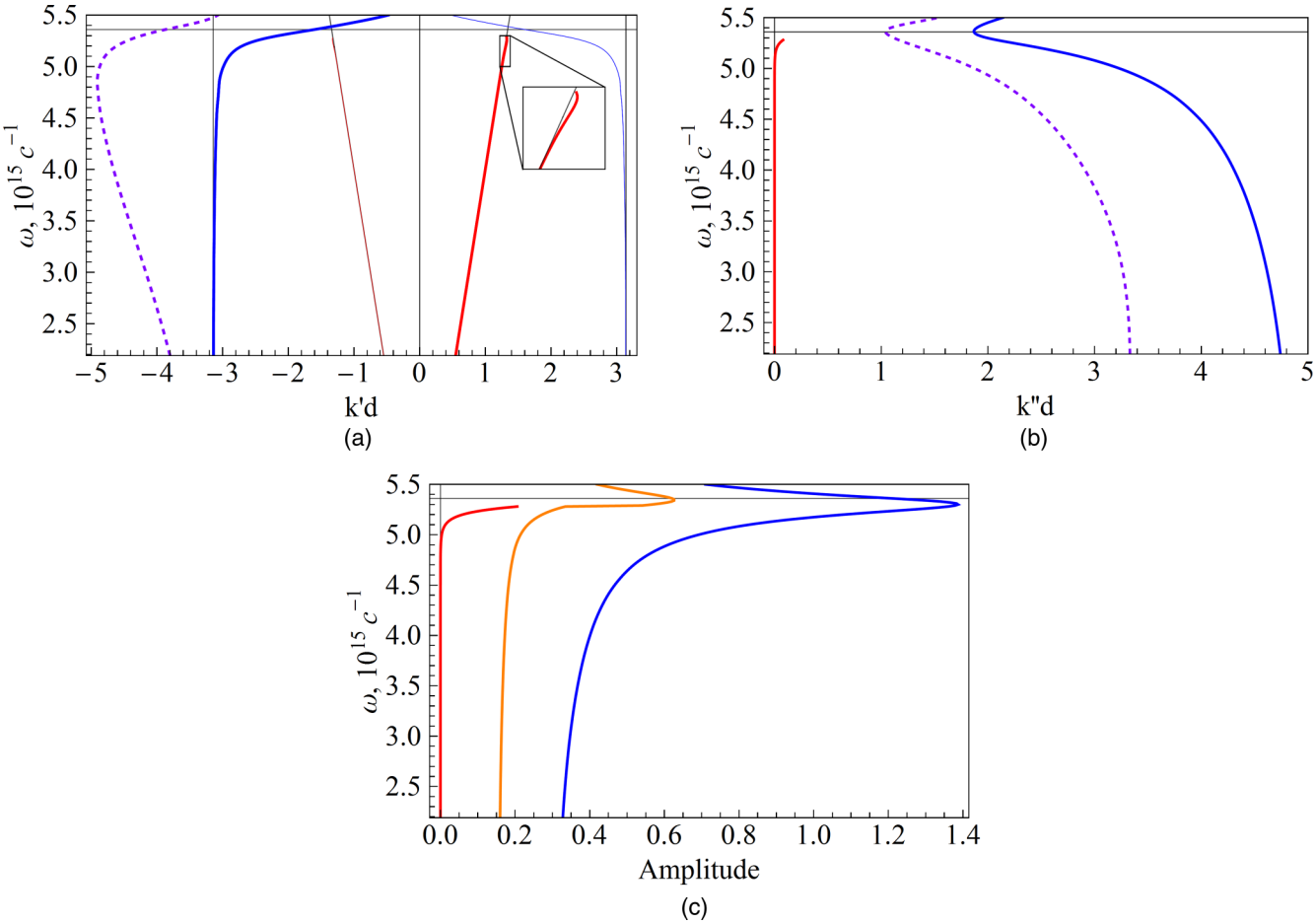

FIG. 3. Dispersion characteristics for the chain of spherical nanoparticles. (a) Dispersion curves. (b) Attenuation constants corresponding to the thick curves in (a). (c) Spectra of excitation efficiency (defined as initial amplitude under the fixed driven field). The spectra are given in the units of total initial amplitude at the resonance frequency. Thick curves correspond to plasmons travelling in the positive direction (identified by a positive imaginary part of the wave number), thin ones in the negative direction. The dispersion curve corresponding to NNA is coplotted by the dashed curve. Blue color is related to the strong plasmon, red to the weak plasmon, orange to the nonexponential contribution. The resonance frequency of a single particle, $\pm\pi$ Brillouin zone boundaries and light lines are depicted by horizontal, vertical, and inclined thin black lines, respectively. The plot range is bounded upwards by the quadrupole resonance frequency of a single particle, where SDA is no longer applicable. The chain period is $d = 75$ nm, radius of a single particle $a = 25$ nm.

plasmon contributions. It means that in a chain of sufficiently long length, it always will dominate the total decay profile far enough from the source. This should not be disregarded, especially given that a nonexponential contribution is easy to be confused with a slowly decaying plasmonic solution.

Numerical solution of the dispersion equation (18) gives dispersion curves [Figs. 3(a) and 3(b)]. The dispersion picture consists of two branches corresponding to two types of plasmons in chains of spherical nanoparticles. The first one is a forward plasmon propagating nearly at the speed of light, which below is called a "weak plasmon." This plasmon has a growing but still very small attenuation constant in a wide frequency range from zero to some critical frequency, the latter being slightly below the plasmonic resonance frequency of a single particle. When this critical frequency is reached, the corresponding pole hides under the cut (see the bottom plots in Fig. 2). This means that the contribution of the pole merges with that of the cut, i.e., this plasmon is no more considered as a distinct solution. The second plasmon is a backward wave, which below is called a "strong plasmon." Plasmons of this type are characterized by a presence of narrow band in the vicinity of the resonance frequency of a single particle, within which the attenuation of the strong plasmon stays relatively small but still higher than that of the weak plasmon.

Comparison of the obtained result with that predicted by the nearest neighbor approximation (NNA) reveals large differences in the dispersion properties. First, NNA predicts existence of only one solution, namely, the strong plasmonlike solution. Second, the dispersion curve of the plasmon predicted by NNA deviates strongly from the full-interaction curve. Third, NNA significantly underestimates actual attenuation of the plasmon.

In addition to dispersion curves, the developed formalism allows us to find decay profiles of plasmons outgoing from a localized source (which is the same as Green's function in the case of a δ-source). These profiles can be calculated directly from Eqs. (15) by numerical integration over the real values of k at each value of n. Individual contributions to a decay

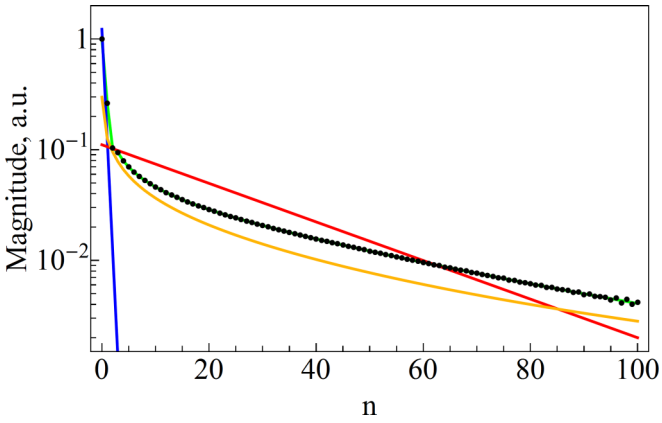

FIG. 4. Decay profiles in the chain of spherical nanoparticles. Points indicate result obtained in a finite chain, green curve shows the decay profile in an infinite chain. Individual contributions are plotted for comparison. Blue color is related to the strong plasmon, red to the weak plasmon, orange to the nonexponential contribution. Frequency is equal to $\omega = 5.31 \times 10^{15}\mathrm{s}^{-1}$.

profile from distinct solutions can be calculated by integration along the corresponding subcontours [e.g., integration along the branch cut in Eq. (19)] or by using Eq. (17).

On the other hand, dipole moments distribution in a finite chain can be found directly from the solution of a finite system of equations [9]. This distribution can be used as a reference for cross-checking of the decay profiles in an infinite chain. As a finite chain problem is a much simpler model that relies on fewer assumptions, this can be considered as a routine test for validation of applicability of the infinite chain approach elaborated here. For this purpose we consider an excitation of a finite chain of $N = 201$ particles numbered from -100 to 100 by a δ-source set at a particle with the number 0.[3] The parameters a and d are taken the same as for the infinite chain. The result of calculation compared to the decay profile obtained for an infinite chain is presented in Fig. 4. Contributions of distinct solutions are also plotted. One can observe a perfect coincidence of both results except a small section near the chain end, where an interference with the reflected wave takes place. Thus, as expected, one can conclude that the developed method does provide an accurate description of modes propagating in a chain of spherical nanoparticles.

The decay profile is formed by a superposition of several separate interfering contributions. Let us consider an excitation efficiency of each contribution for better understanding the role of each of them in the waveguide. This can be done by calculating the initial amplitude of each contribution (amplitude at $n = 0$) using Eqs. (15) and (17) in a similar way as in calculating the decay profiles. Frequency dependence of such amplitudes at a fixed value of external field is shown at Fig. 3(c).

[3]Such a choice is conditioned by the intention to get rid of boundary effects. The result of calculation would be sufficiently different if the source would be set, for example, at the chain end.

First, one can see from the figure that all the three contributions have a maximum in their excitation spectra near the resonance frequency of a single particle. Second, the initial amplitudes of different contributions have different scales. The backward plasmon has the largest initial amplitude in the whole frequency range. For this reason it is referred to as "strong." The forward plasmon, in contrast, has the least initial amplitude, and is referred to as "weak." The initial amplitude of the nonexponential wave is between these two values. The jump in the non-exponential wave amplitude is due to the joining of the nonexponential wave and weak plasmon into a single solution, which corresponds to the hiding of the pole under the brunch cut mentioned above.

Thus, the response of the spherical nanoparticle chain to a point stationary source can be represented as a sum of three contributions, which can be characterized separately, namely, two plasmons (representing a discrete spectrum) and additional non-plasmonic contribution, which is not described by a single wave number (representing a continuous spectrum). As a result, the dispersion equation for the plasmonic waves is obtained, which coincides with that obtained in Refs. [4,12,28]. The main outcomes of the provided theory are the excitation spectra of the separate contributions and possibility to compare the plasmonic and non-plasmonic contributions at any distance from the source. The obtained data provide all basic information about the guiding properties of the chain helpful for further qualitative analysis. Two possible directions of such an analysis are search for optimal operating frequency and determination of the most suitable type of plasmon to be utilized for energy transfer in a specific waveguide.

In this way, a comprehensive approach to the study of spherical nanoparticle chains described above has been developed elsewhere [4,12,28]. However, such study of solutions excited in chains made up of complex-shaped nanoparticles is still unavailable. In the next section, we generalize the theory given above to the case of chains of nanoparticles of an arbitrary shape including method of finding dispersion and providing all the related analysis.

IV. WAVES IN CHAINS OF NANOPARTICLES OF COMPLEX SHAPE

The approach developed to the study of plasmons in chains of spherical nanoparticles cannot be straightforwardly adapted for the work with chains of particles of an arbitrary shape. Plasmonic oscillations in such particles can be significantly distorted from those in a dipole mode of spherical particles, so that SDA in no more applicable [31]. Instead, these oscillations should be described by spatial charge and current distributions. Therefore, the interaction between the chain elements is not described analytically, and the continuation into the complex plane is not straightforward. Below we show how to operate in this case.

As an example, we consider an axial chain of split-ring resonators (SRRs, see. Fig. 5). SRRs are popular elements in optical and microwave plasmonics [32–35]. It was shown that chains made up of SRRs support plasmonic waves travelling along the chain [6,21].

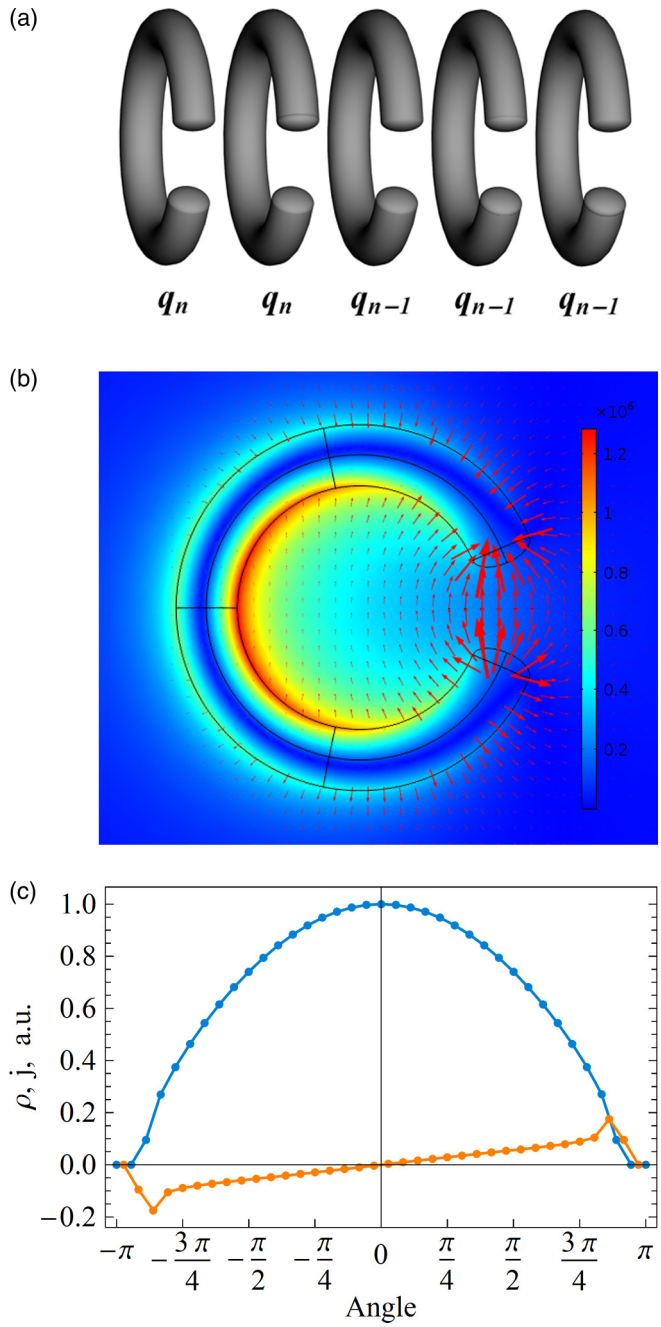

FIG. 5. (a) Geometry of the SRR chain. (b) Magnetic (shown by color) and electric (shown by arrows) field distribution in the magnetodipole mode of SRR single particle. (c) Current (upper curve) and charge (lower curve) angular distribution in a single SRR in the filamentary current approximation.

A. Description of single SRR plasmonic particle

The geometrical model of the SRR particle is a solid torus with major and minor radii [36] being equal to $R = 100$ nm and $r = 20$ nm, respectively, and with a 0.8 radian gap. The ends of the resonator are rounded by the two half-ellipsoidal stubs with semi-axes lengths of r, r, and $r/2$ [see Fig. 5(b)]. The material of the particle is silver, which permittivity is taken from the experimental data obtained by Babar [27].

A single SRR exhibits a series of plasmonic eigenmodes. The ground mode is magnetodipole and the second mode is electrodipole [37]. The magnetodipole mode is the most interesting one [38], and it is spectrally separated from the other modes due to the split-ring geometry. Particularly, this mode has nearly twice smaller frequency than the electrodipole mode. Therefore, in a wide frequency range around the ground mode eigenfrequency, it can be treated as the sole mode contributing to guidance. Within this single-mode approximation, charge oscillations in a single particle can be described by a single generalized coordinate q, which we define as an instantaneous charge of a half of the particle.

To investigate the SRR eigenmodes we solve an eigenvalue problem by means of COMSOL Multiphysics. The simulation provides the complex values of eigenfrequencies. At our parameters, these values are $\hat{\omega}_0 = (9.66 \times 10^{14} + 1.57 \times 10^{13} i)\ \mathrm{s}^{-1}$ for the magnetodipole mode and $\hat{\omega}_1 = (1.97 \times 10^{15} + 1.58 \times 10^{14} i)\ \mathrm{s}^{-1}$ for the electrodipole mode. The angular charge and current distributions characteristic of each mode can also be extracted from the simulation data. The magnetodipole mode characteristic distributions are shown at Fig. 5(b).

According to a circuit model approximation [39], generalized coordinate of magneto-dipole oscillations in a single particle obeys the equation

$$\ddot{q}(t)L + \dot{q}(t)R + q(t)/C = V(t),$$

where L, R, and C are the effective values of the particle inductance, resistance, and capacitance, respectively, $V(t)$ is an external electromotive force. Introducing conventional notifications for the eigenfrequency and damping coefficient, $\omega_0 = 1/(LC)$ and $\gamma = R/2L$, the equation can be rewritten in the form

$$\ddot{q}(t) + 2\gamma\dot{q}(t) + \omega_0^2 q(t) = V(t)/L.$$

The parameters γ and ω_0 can be derived from the complex eigenfrequency $\hat{\omega}_0$ of the magnetodipole mode as $\omega_0 = |\hat{\omega}_0|$, $\gamma = \mathrm{Im}(\hat{\omega}_0)$. Self-inductance of the SRR can be approximately calculated from the relation [40]

$$L = \mu_0 R\left(\ln\left(\frac{8R}{r}\right) - \frac{7}{4}\right).$$

B. SRR coupling

When proceeding from a single SRR particle to a chain of SRRs, one must introduce inter-particle interaction. It can be described in terms of mutual capacitance K and mutual inductance M. Total electromotive force (emf) applied to the nth particle from a mth one is

$$V_{nm} = -M_{nm}\ddot{q}_m - K_{nm}^{-1} q_m.$$

As in the case of interaction between the spherical particles, due to translational invariance emf does not depend on each n and m separately, but only on their difference. Thus, further in the text, notations K_m, M_m, V_m, etc. with one subscript are used, which means interaction of two SRRs separated by a distance of m periods. Corresponding notifications without subscripts stand for the same values considered as continuous functions of distance, i.e., $K_m = K(md)$, with d being the period of the chain.

Coupling coefficients K and M can be calculated using the following overlap integrals [41]:

$$K^{-1} = \frac{1}{4\pi\varepsilon_0}\iint \frac{\rho(\vec{r_1})\rho(\vec{r_2})e^{ik_0|\vec{r_1}-\vec{r_2}|}}{|\vec{r_1}-\vec{r_2}|}dr_1dr_2, \quad (20)$$

$$M = \frac{\mu_0}{4\pi}\iint \frac{j(\vec{r_1})j(\vec{r_2})e^{ik_0|\vec{r_1}-\vec{r_2}|}}{|\vec{r_1}-\vec{r_2}|}d\vec{r_1}d\vec{r_2}. \quad (21)$$

Here, $\rho(\vec{r})$ and $j(\vec{r})$ are the dimensionless charge and current angular distributions of the interacting SRRs, respectively. In the approximation of thin and distant enough SRRs, a filamentary current model is applicable and these distributions can be replaced by one-dimensional angle distributions shown in Fig. 5(c). They are normalized in such a way that the total dimensionless charge of a half of each SRR and dimensionless current in its center are set to unity.

The oscillation equation of the entire chain is thus written in the form

$$\ddot{q}_n + 2\gamma\dot{q}_n + \omega_0^2 q_n = -\sum_{m\neq n}\left(K_{nm}^{-1}q_m + M_{nm}\ddot{q}_m\right)/L + V_n^{\text{ext}}/L,$$

or, assuming the time dependence $q_n(t) = q_{0n}\exp(-i\omega t)$, one obtains

$$\left(-\omega^2 - 2i\gamma\omega + \omega_0^2\right)q_n = \sum_{m\neq n}\left(\omega^2 M_{nm} - K_{nm}^{-1}\right)q_m/L + V_n^{\text{ext}}/L.$$

After the introduction of the notations,

$$\alpha = \left(-\omega^2 - 2i\gamma\omega + \omega_0^2\right)^{-1}, \quad g_{nm} = \left(\omega^2 M_{nm} - K_{nm}^{-1}\right)/L, \quad (22)$$

the latter equation reduces to the form that is equivalent to Eq. (1),

$$q_n = \alpha\sum_{m\neq n} g_{nm}q_m + \alpha V_n^{\text{ext}}/L. \quad (23)$$

Here, α is a SRR particle response function, which is analogous to the polarizability $\alpha^{(s)}$ of a spherical particle in Eq. (1), although it has a different dimension. Function g_{mn} that characterizes the interaction between SRRs is, in turn, analogous to $g_{mn}^{(s)}$. Finally, the term V_n^{ext}/L, which expresses the external excitation of the chain of SRRs, plays the same role as the external field E_n^{ext} in the chain of spherical nanoparticles.

Using this similarity, one can perform the same sequence of operations that was shown in the Sec. III to obtain the dispersion equation. The crucial difference between Eqs. (1) and (23) in this regard is that spherical particles interaction function $g_{nm}^{(s)}$ is based on inverse-power series that allows us to perform summation procedure using the definition of polylogarythms [see Eqs. (10) and (11)], whereas SRR function g_{nm} is found numerically and does not have any analytical representation. Thus, to complete the reduction of Eq. (23) to Eq. (1), one should replace g_{nm} by an inverse-power series.

C. Approximation of interaction function

The general feature of complex-shaped nanoparticles is that they exhibit complex-shaped charge distribution resulting in interparticle interaction function that does not have an analytical representation. One can still calculate it numerically in an arbitrary number of points. In case of SRRs, we can use the filamentary current model for this purpose yielding integral representation Eqs. (20) and (21) for the coupling coefficients. Here we show how such complex-shaped nanoparticles' interaction function can be approximated by an analytic representation to derive the dispersion relations.

Due to the retardation effects, interaction function $g(l)$ (we imply the relation $g_{mn} = g_{m-n} = g(|m-n|d)$) rapidly oscillates with distance. It is appropriate to distinguish an oscillating factor to facilitate the approximation procedure,

$$g(l) = \bar{g}(l)e^{ik_0 l}.$$

The slowly varying function $\bar{g}(l)$ can then be approximated by an inverse power series. This function exhibits fast growth near zero and asymptotically tends to zero with the increasing distance, so one can suggest that a few series terms would be required for accurate enough approximation. The resulting approximant is thus given in the form

$$g_m \approx \left(\frac{A_1}{|md|} + \frac{A_2}{|md|^2} + \frac{A_3}{|md|^3} + \frac{A_4}{|md|^4} + \ldots\right)e^{ik_0 d|m|} = \left(\sum_{s=1}^{N}\frac{A_s}{|md|^s}\right)e^{ik_0 d|m|}. \quad (24)$$

When comparing Eq. (2) to Eq. (24), one can see that the former is the particular case of the latter with $A_1 = k_0^2/(4\pi\varepsilon_0)$, $A_2 = ik_0/(4\pi\varepsilon_0)$, and $A_3 = -1/(4\pi\varepsilon_0)$ and other approximating coefficients equal to zero. Assuming approximant in the form of Eq. (24) and substituting it into Eq. (23) one can complete the derivation of the dispersion equation in the same way as it was done in the case of spherical nanoparticles chain. The resulting dispersion equation is

$$1 - \alpha\Sigma(k) = 0, \quad (25)$$

with

$$\Sigma(k) = \sum_{s=1}^{N}\frac{A_s}{d^s}\left[\text{Li}_s(e^{i(k_0+k)d}) + \text{Li}_s(e^{i(k_0-k)d})\right]. \quad (26)$$

By analyzing these expressions, one can see that the obtained dispersion equation is identical to Eq. (18) and $\Sigma(k)$ is basically a generalization of $\Sigma^{(s)}(k)$ in Eq. (11). Thus, in a chain of complex-shaped nanoparticles, the approximation of interaction function by the inverse power series Eq. (24) provides the reduction of the whole formalism to that appearing in the investigation of the spherical nanoparticles chain. As the form of approximant Eq. (24) does not specify the exact physical properties of the particles such as shape, size, material, or mutual orientation, this approach is applicable to an arbitrary particle chain. Such specification is achieved through particular values of approximation coefficients $A_1, A_2, A_3, \ldots$ So, to obtain dispersion relations in the SRR chain from the dispersion equation (25) we must determine the concrete values of the approximation coefficients for the interaction function in the case of SRRs.

D. Approximation coefficients

In the present work, coupling coefficients K^{-1} and M entering the definition of interaction function are approximated separately by the two inverse power series with distinguished exponential oscillating factor,

$$K^{-1}(l) \approx \left(\frac{B_1}{l} + \frac{B_2}{l^2} + \frac{B_3}{l^3} + \frac{B_4}{l^4} + \ldots\right) e^{ik_0 l} = \left(\sum_{s=1}^{N} \frac{B_s}{l^s}\right) e^{ik_0 l}, \tag{27}$$

$$M(l) \approx \left(\frac{C_1}{l} + \frac{C_2}{l^2} + \frac{C_3}{l^3} + \frac{C_4}{l^4} + \ldots\right) e^{ik_0 l} = \left(\sum_{s=1}^{N} \frac{C_s}{l^s}\right) e^{ik_0 l}. \tag{28}$$

This will result in g approximant in the form of Eq. (24) with the following approximation coefficients:

$$A_s = \frac{\omega^2 C_s - B_s^{-1}}{L}. \tag{29}$$

The values of K^{-1} and M for approximation are evaluated by Eqs. (20) and (21) in the nodes of the approximation grid l_i. Every value of K^{-1} and M is then divided by $\exp(ik_0 l_i)$ to numerically distinguish the oscillating factor.

Search for the optimum approximants is done by adjusting all the approximation coefficients B_s and C_s to minimize the following total relative discrepancies Δ_K and Δ_M,

$$\Delta_K = \sum_i \frac{\left|K^{-1}(l_i)\exp(-ik_0 l_i) - \sum_{s=1}^{N} B_s / l_i^s\right|^2}{|K^{-1}(l_i)|^2}, \tag{30}$$

$$\Delta_M = \sum_i \frac{\left|M(l_i)\exp(-ik_0 l_i) - \sum_{s=1}^{N} C_s / l_i^s\right|^2}{|M(l_i)|^2}. \tag{31}$$

Note that $K^{-1}(l)\exp(-ik_0 l)$ and $M(l)\exp(-ik_0 l)$ are numerical slowly varying functions of l.

Let us outline a few features of the optimization problem Eqs. (30) and (31) that are important for the successful implementation of the approximation procedure. First, as absolute values of K^{-1} and M at large l may be up to several orders of magnitude smaller than that at $l \sim 1$, a relative discrepancy should be used instead of the absolute discrepancy to avoid overweight of short-range grid nodes. Second, as K^{-1} and M change rapidly at small distances and become more smooth at larger ones, a logarithmic grid l_i should be used for uniform nodes weighting at both short and long distances. Third, due to limitations of filamentary current approximation, the short end of the approximation grid should not be closer than $l = 1$. Fourth, the far end of the grid should be taken far enough so that the minor contributions into the interaction function, which decay slowly, are revealed. Fifth, it should be noted that the lowest order term in the K^{-1} approximant corresponds to $i = 2$, whilst the first term B_1 is identically equal to zero because of the symmetry of the magneto-dipole mode and the geometry of the problem.

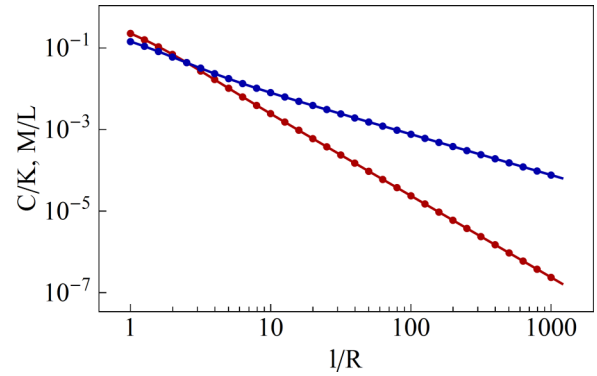

FIG. 6. The absolute value of the electric (red) and magnetic (blue) interparticle interaction terms calculated numerically (dots) and the result of inverse-power series approximation Eqs. (27) and (28) with $N = 7$ (solid curves).

With this in mind, we use a grid of 31 nodes logarithmically distributed from $l_1 = 1$ to $l_{31} = 1000$ and set $B_1 = 0$ constantly upon the approximation. The result of approximation is shown in Fig. 6.

The remaining free parameter that was not discussed so far is the number of approximation terms N. One can suggest that more terms provide more accurate approximation. Based on this, the whole approximation process in the present work is organized iteratively, with N increasing by 1 at each step starting from $N = 4$. At each step, the optimization problem Eqs. (30) and (31) is solved using the Newton's method. The resulting values of the approximation coefficients B_s and C_s are then used as initial values at the next step. For those coefficients which firstly appear at the current step, zero is used as the initial value. At the first step, the search is also started from all the coefficients equal zero. The resulting values of B_s and C_s are substituted into Eq. (29) to specify the function $\Sigma(k)$ to use in the dispersion equation. The dispersion equation can then be handled in the same manner as it was done with the dispersion equation of the spherical nanoparticles chain Eq. (18), resulting in the dispersion curves of SRR particles chain. Different dispersion pictures corresponding to different values of N are shown in Fig. 7.

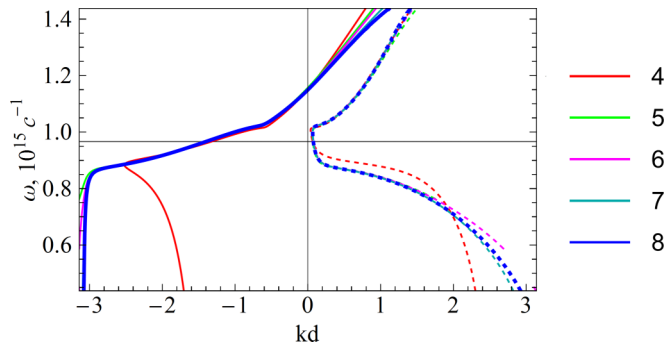

FIG. 7. Dispersion curves of the strong plasmon in the SRR chain calculated at different numbers N of approximation terms in Eqs. (27) and (28).

We suggest an increasingly good approximation when increasing N and expect that the sequence of dispersion curves converges to some limit state that can be considered as a true dispersion picture. The convergence process is shown in Fig. 7 with the dispersion curve of the strong plasmon as an example. One observes that the convergence does practically occur by the $N = 8$ iteration. The similar situation can be observed with a weak plasmon dispersion curve (not shown). In the further discussion, the result obtained with $N = 7$ terms is taken as the final result. At larger values of N, the search for the optimum values of B_s and C_s leads ho high numerical errors, which appear as a noise in the resulting dispersion curves (see the next Section for details).

The dispersion picture consists of two branches corresponding to plasmons of the same two types that exist in chains of spherical nanoparticles, i.e., the strong and the weak plasmons. Their general features remain the same. However, due to the fact that the SRR chain demonstrates lower losses than the spherical particle chain, one can observe that the curves behave in concert clinging together and then splitting apart below some characteristic frequency [1.02×10^{15} s^{-1} in Fig. 8(a)].[4] Such a behavior is well known for the SPP running along thin metal films (see, e.g., Fig. 7(b) in Ref. [42]). It also has already been demonstrated and discussed in the chain of unrealistically low-loss metallic spherical particles [28]. This leads to the appearance of a clearly defined band structure, wherein the strong plasmon has a transmittance band about the resonance frequency with an upper boundary occurring at the characteristic frequency, and the weak plasmon follows the light line until approaching the characteristic frequency, where its attenuation drastically increases. It is interesting to note that the strong plasmon attenuation is now significantly lower, while the attenuation of the weak plasmon is, in contrast, higher than those in the spherical particle chain.

Comparing the obtained result to that predicted by NNA, one can observe large differences in the dispersion properties, similar to those in case of spherical particles chain. First, NNA predicts existence of only one solution, namely, the strong plasmon-like solution [Fig. 8(a)]. Second, the dispersion curve of the plasmon predicted by NNA always remains in the left half of the first Brillouin zone, while the full-interaction curve intersects the frequency axis. Third, the behavior of k'' within the transmittance band differs substantially [Fig. 8(b)].

Decay profiles of in the infinite SRR chain can be calculated using the formula

$$q_n = \frac{1}{2\pi} \int_{\mathbb{R}} \frac{\alpha \exp\left(ik(n-m)\right)}{1 - \alpha \Sigma(k)} dk, \tag{32}$$

which is derived from Eq. (23) similarly to the derivation of Eq. (15) from Eq. (1). Here, α and $\Sigma(k)$ are defined by Eqs. (22) and (26), respectively.

[4]Since polylogarithm is a multi-valued function, a pole may move away from the principal branch to another one through a branch cut (corresponds to a dispersion curve hitting the right light line). To shift the cut and build the continuation of the curve, one can use a relation between the values of polylogarithm at the upper and lower branches, $\mathrm{Li}_s(x) \to \mathrm{Li}_s(x) \pm 2\pi i \ln^{s-1}(x)/\Gamma(s)$.

Now we perform the validation procedure described in the previous Section through cross-checking the obtained results with that in a finite chain. For this purpose we consider an excitation of a finite SRR chain of $N = 201$ particles numbered from -100 to 100 by a δ-source set at a particle with the number 0.[3] The problem is solved by the same standard method that was used in the case of finite spherical particle chain problem (see the explanations to Fig. 9) [6,9]. The result of calculation compared to the decay profile obtained in an infinite chain is shown in Fig. 9. Contributions of distinct solutions are also plotted. One can observe a perfect coincidence of both results including complicated interference effects between distinct solutions. The exception is a small section near the chain end, where an interference with a reflected wave takes place. Thus, one can conclude that the developed method does provide a highly accurate description of modes propagating in the SRR chain.

Let us consider an excitation efficiency of each contribution to the decay profile. Frequency dependence of such efficiencies defined as initial amplitudes (amplitudes at $n = 0$) of corresponding solutions under the fixed driven field is shown in Fig. 8(c). It can be seen that excitation spectra become more sophisticated being compared with those in case of spherical particle chain [Fig. 3(c)]. Due to low losses in the SRR chain the plots corresponding to the strong and to the weak plasmons exhibit the following behavior. Above some characteristic frequency, at which the dispersion curves are clinging together, the initial amplitudes of the strong and the weak plasmons also become almost the same. Below this frequency, the amplitudes are different. The initial amplitude of the strong plasmon is still higher than that of the weak plasmon in the whole frequency range (that justifies their denotations). However, the intermediate position of the nonexponential wave is no longer preserved. The excitation spectrum of the strong plasmon now exhibits two distinct peaks at the boundaries of the transmittance band. The peak exhibited by the weak plasmon is also shifted up from the resonance frequency to the characteristic frequency. The jump in the nonexponential wave amplitude is due to the joining of the nonexponential wave and the weak plasmon into a single solution.

Thus, the proposed approach for the characterization of plasmons propagating in complex-shaped nanoparticle chains provides a highly accurate modes description and opens up a wide spectrum of analysis that was previously available only for spherical particles chains. Since the key point of the approach, which consists in the approximation of the interaction function with the inverse-power series and subsequent analytical continuation to the complex wave-number values, is universal and is not restricted to the considered particles' geometry, the approach developed here can be applied to a chain made up of particles of any arbitrary shape.

E. Accuracy and limitations

Here we discuss possible issues with convergence of the dispersion curves that should be handled with to successfully achieve a satisfactory approximation and avoid misinterpretation of the results.

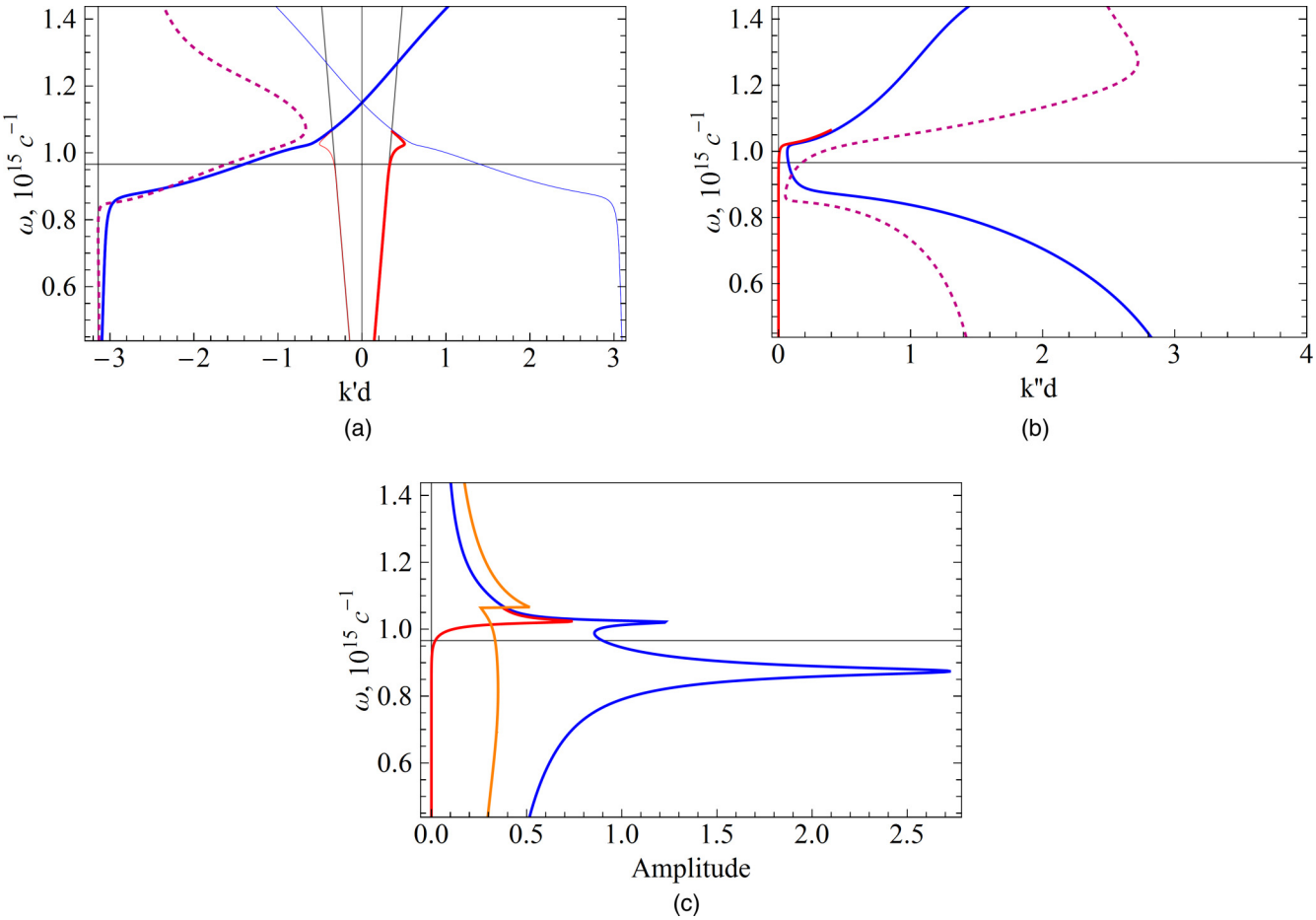

FIG. 8. Dispersion characteristics for the chain of SRRs. (a) Dispersion curves. (b) Attenuation constant. (c) Spectra of excitation efficiency (defined as initial amplitude under the fixed driven field). The spectra are given in the units of total initial amplitude at the resonance frequency. Thick curves correspond to plasmons travelling in the positive direction (identified by a positive imaginary part of the wave number), thin ones in the negative direction. The dispersion curve corresponding to NNA is coplotted by the dashed curve. Blue color is related to the strong plasmon, red to the weak plasmon, orange to the nonexponential contribution. The resonance frequency of a single particle, $\pm\pi$ Brillouin zone boundaries, and light lines are depicted by horizontal, vertical, and inclined thin black lines, respectively. The plot range is bounded upwards far enough from the electrodipole resonance frequency of a single SRR particle that restricts applicability of single mode approximation.

1. False solutions

In the case of spherical particle chain, the dispersion equation (18) contains the function $\Sigma^{(s)}(k)$ that includes a series of three strictly specified terms. Solving the dispersion equation results in exactly three types of propagating waves, namely, the strong and weak plasmons corresponding to the two poles at the complex k-plane and a nonexponential wave corresponding to a branch cut. In the case of complex-shaped particle chain, the dispersion equation (25) contains the function $\Sigma(k)$ that includes a series of terms whose number and coefficient values may vary depending on the approximation order N in Eq. (24). However, one may find larger number of the dispersion equation solutions, which results in the existence of more than two poles, producing more than two branches in the dispersion picture. Two of them still can be recognized as corresponding to weak and a strong plasmons, but other ones exhibit some chaotic behavior. The number of this additional poles can be different depending on the number of approximation terms N and increases with increasing N. All of these solutions have large wave-number imaginary parts ($k'' \gg 1$), indicating that these plasmons are highly damped. To interpret this result we consider the total decay profiles with the weak and strong plasmons and non-exponential wave contributions being subtracted. We take a profile previously calculated in the finite chain (see Fig. 9) as the "true decay profile," then subtract the said contributions in infinite chain and consider the remainder (i.e., the discrepancy between the finite and infinite chain solutions). Ideally, this remainder must be zero, meaning that the decay profile in a finite chain must break entirely into the contributions analytically found from the infinite chain problem. But due to inaccuracies the discrepancy actually remains at the level of 0.001 of the initial amplitude (see Fig. 10). However, one can see that the discrepancy rises sharply in the neighborhood of the δ-source reaching a value of 0.1. But then if we also sequentially subtract contributions of the two additional plasmonlike solutions appearing in the considered example, the remainder will return again to the average level. Therefore, these additional plasmonlike solutions can be perceived as a mathematical artifact of the method arising from numerical inaccuracies but not as a

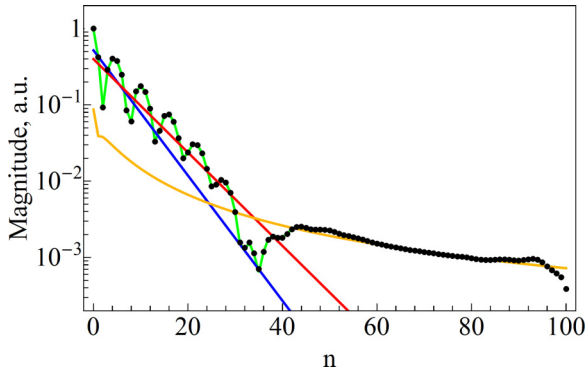

FIG. 9. Decay profiles in the SRR chain. Points indicate result obtained in a finite chain, green curve shows the decay profile in an infinite chain. Individual contributions are plotted for comparison. Blue color is related to the strong plasmon, red to the weak plasmon, orange to the nonexponential contribution. Frequency $\omega = 1.028 \times 10^{15} \mathrm{s}^{-1}$.

physically existing phenomenon. Numerically, it manifests in a few percent discrepancy between the full decay profile in an infinite chain (taken as a sum of weak and strong plasmons and non-exponential wave) and the solution found in finite chain. However, due to high damping, this discrepancy is noticeable only at short distances and comes to naught a few particles aside from the δ-source.

Nevertheless, since the amplitudes of the false solutions are considerable in the neighborhood of the δ-source, they should not be neglected when calculating the excitation spectra, which are defined through the amplitudes at the zeroth particle. In this paper, we include the contributions of the false solutions into the nonexponential wave decay profile that may result in a few percent normalization inaccuracy in Fig. 8(c).

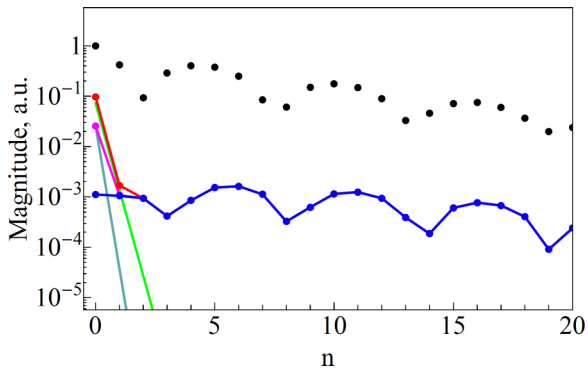

FIG. 10. The remainder of the total decay profile after sequential subtraction of different contributions. The full solution in the finite chain is shown by black points. At the first step, the weak and strong plasmons and non-exponential wave contributions are subtracted from the full solution (red points). At the second step, one of the two false solutions is subtracted (magenta points). At the third step, the last false solution is subtracted (blue points). Green and aquamarine points show the contributions of the false solutions. The frequency is $\omega = 1.028 \times 10^{15} \mathrm{s}^{-1}$.

2. Numerical noise

Besides the mentioned difficulties, let us mention one more issue, which addresses the choice of the number N of terms in Eq. (24). Search for the optimal set of approximation coefficients B_s and C_s in a multidimensional space is a computationally hard task. At high N, it cannot be solved precisely by the computational algorithm due to emergence of local minima and high computational time. This leads to the fact that the optimization problem Eqs. (30) and (31) could not be solved for an arbitrarily large N. In practice, starting from $N = 9$ we observe the growth of numerical errors. The noise affects primarily the solutions with high imaginary part of k, i.e., the false solutions discussed above and the strong plasmon far from the transmittance band. Nonetheless, as was mentioned earlier, in our case $N = 7$ terms are enough to consider the dispersion curves obtained at that step converged to the "true" dispersion.

V. CONCLUSIONS

We have proposed an approach for description of plasmons in chains of nanoparticles of a complex shape. This approach leads to finding the dispersion relations, decay profiles and excitation spectra. The approach is basically a generalization of the method previously developed by Koenderink for spherical nanoparticle chains [4]. We have shown how the complex-shaped nanoparticles interaction functions that are known only numerically can be approximated by the inverse power series with subsequent analytical continuation to the complex wave numbers.

We applied the developed method to a chain made up of split-ring resonators and compared the results to that in a spherical nanoparticle chain. We found that a localized source excites three contributions, namely, two plasmonic solutions and a non-exponential wave. All three types are common for both spherical and SRR particle chains.

The first plasmonic solution ("strong plasmon") originates from the plasmon localized at a single particle, which is a magnetic mode of SRR in our case. This solution is formed by the strong coupling mechanism. It can be described with the account of only nearest neighbor interactions, although this brings considerable mistakes into the dispersion relation. This plasmon is mostly a backward wave. The strong plasmon has the largest decay among the three contributions. It appears that most papers on nanoparticles chain waveguides imply this type of plasmon as a signal or energy carrier.

The second plasmonic solution ("weak plasmon") appears with the account of the radiative part of nanoparticles' field. It requires the account of many interparticle interactions. The dispersion curve follows the light line; therefore, the wave is mostly forward. The wave has a very large propagation length.

The third, nonexponential contribution, strictly speaking, is not an eigensolution, because it does not have any characteristic shape in a sense that the latter depends on the form of the source. It cannot be described by a certain complex wave number and includes many harmonics. Nonexponential contribution is often referred to as the continuous spectrum in contrast with the discrete spectrum, which is presented by the plasmonic solutions in our system.

When the chain is excited by a source, the response may be represented as a sum of the three mentioned contributions. The strong plasmon is the strongest near the source, but it decays just near the source. The weak plasmon is characterized by smaller initial amplitude and lower damping. Far enough from the source, a complete solution consists almost entirely of the nonexponential wave, which is due to a nonexponential form of the decay profile.

If one compares a chain of spherical particles to that of SRRs, the latter are far less dissipative. In particular, the plasmonic dispersion curves in the SRR chain clearly form a single dispersion structure similar to that in thin metallic films [42], whereas this picture is deformed unrecognizably in spherical particle chains due to too high dumping.

We also found that the excitation spectrum of the strong plasmon is not uniform within the transmittance band. Instead, it has two distinct peaks at its boundaries (this effect is also blurred in the spherical nanoparticle chain due to high dumping). Due to this effect, when designing a nanoparticle chain waveguide, the optimal operational frequency may occur somewhere aside from the resonanse frequency, contrary to a widespread approach, where the resonance frequency is treated as an optimal frequency for signal propagation.

Basically, the key point of the proposed method is the approximation procedure, which doesn't depend on the particles' geometry, material or orientation as well as on the nature of the considered wave at all. So, this method can also be adapted to chains of magnonic particles, metamaterial meta-atoms etc. Therefore, the proposed approach is universal for studying chain waveguides of various kinds.

ACKNOWLEDGMENTS

The work was supported by the Advanced Research Foundation (Contract No. 7/004/2013-2018 on 23.12.2013). Y.E.L. acknowledges Russian Science Foundation under Grant No. 17-12-01393.

[1] M. Quinten, A. Leitner, J. Krenn, and F. Aussenegg, Opt. Lett. **23**, 1331 (1998).
[2] S. A. Maier, *Plasmonics: Fundamentals and Applications* (Springer Science & Business Media, Berlin, 2007).
[3] D. Citrin, Opt. Lett. **31**, 98 (2006).
[4] A. F. Koenderink and A. Polman, Phys. Rev. B **74**, 033402 (2006).
[5] E. D. Chubchev, A. V. Dorofeenko, and A. P. Vinogradov, J. Commun. Technol. Electron. **63**, 850 (2018).
[6] E. Shamonina, V. Kalinin, K. Ringhofer, and L. Solymar, J. Appl. Phys. **92**, 6252 (2002).
[7] S. A. Maier, P. G. Kik, and H. A. Atwater, Phys. Rev. B **67**, 205402 (2003).
[8] V. Lomanets, O. Zhuromskyy, G. Onishchukov, O. Sydoruk, E. Tatartschuk, E. Shamonina, G. Leuchs, and U. Peschel, Appl. Phys. Lett. **97**, 011108 (2010).
[9] W. H. Weber and G. W. Ford, Phys. Rev. B **70**, 125429 (2004).
[10] D. Citrin, Nano Lett. **4**, 1561 (2004).
[11] K. H. Fung and C. T. Chan, Opt. Lett. **32**, 973 (2007).
[12] A. Alu and N. Engheta, Phys. Rev. B **74**, 205436 (2006).
[13] I. B. Udagedara, I. D. Rukhlenko, and M. Premaratne, Phys. Rev. B **83**, 115451 (2011).
[14] S. Campione, S. Steshenko, and F. Capolino, Opt. Express **19**, 18345 (2011).
[15] H.-Y. Chen, C.-L. He, C.-Y. Wang, M.-H. Lin, D. Mitsui, M. Eguchi, T. Teranishi, and S. Gwo, ACS Nano **5**, 8223 (2011).
[16] B. Shen, Y. Huang, X. Duan, X. Ren, X. Zhang, Q. Wang, and D. Zhang, Appl. Opt. **51**, 6376 (2012).
[17] T. Li, R. Ye, C. Li, H. Liu, S. Wang, J. Cao, S. Zhu, and X. Zhang, Opt. Express **17**, 11486 (2009).
[18] H. Liu, D. A. Genov, D. M. Wu, Y. M. Liu, J. M. Steele, C. Sun, S. N. Zhu, and X. Zhang, Phys. Rev. Lett. **97**, 243902 (2006).
[19] H. Liu, T. Li, Q. J. Wang, Z. H. Zhu, S. M. Wang, J. Q. Li, S. N. Zhu, Y. Y. Zhu, and X. Zhang, Phys. Rev. B **79**, 024304 (2009).
[20] S. Wang, T. Li, H. Liu, F. Wang, S. Zhu, and X. Zhang, Opt. Express **16**, 3560 (2008).
[21] E. Shamonina, V. Kalinin, K. Ringhofer, and L. Solymar, Electron. Lett. **38**, 371 (2002).
[22] See Supplemental Material at http://link.aps.org/supplemental/10.1103/PhysRevB.98.085134 for illustration of the failure of several nearest-neighbor approximations.
[23] A. Pikalov, A. Dorofeenko, A. Granovsky, and Y. E. Lozovik, J. Commun. Technol. Electron. **63**, 189 (2018).
[24] C. F. Bohren and D. R. Huffman, *Absorption and Scattering of Light by Small Particles* (John Wiley & Sons, New York, 2008).
[25] F. Capolino, *Theory and Phenomena of Metamaterials* (CRC press, Boca Raton, 2009).
[26] H. Van de Hulst, *Light Scattering by Small Particles* (Dover Publications, New York, 1981).
[27] S. Babar and J. Weaver, Appl. Opt. **54**, 477 (2015).
[28] K. H. Fung, R. C. H. Tang, and C. Chan, Opt. Lett. **36**, 2206 (2011).
[29] M. Abramowitz and I. A. Stegun, *Handbook of Mathematical Functions with Formulas, Graphs, and Mathematical Table* (Dover, New York, 1965), Vol. 2172.
[30] V. A. Markel and A. K. Sarychev, Phys. Rev. B **75**, 085426 (2007).
[31] E. Chubchev and A. Vinogradov (unpublished).
[32] M. Decker, R. Zhao, C. Soukoulis, S. Linden, and M. Wegener, Opt. Lett. **35**, 1593 (2010).
[33] B. Lahiri, A. Z. Khokhar, M. Richard, S. G. McMeekin, and N. P. Johnson, Opt. Express **17**, 1107 (2009).
[34] R. Marques, J. Martel, F. Mesa, and F. Medina, Phys. Rev. Lett. **89**, 183901 (2002).
[35] F. Martin, F. Falcone, J. Bonache, R. Marques, and M. Sorolla, IEEE Microw. Wirel. Compon. Lett. **13**, 511 (2003).
[36] L. Ma, Z. Hu, X. Liang, Z. Meng, and Y. Hu, Appl. Opt. **49**, 1979 (2010).
[37] C. Rockstuhl, F. Lederer, C. Etrich, T. Zentgraf, J. Kuhl, and H. Giessen, Opt. Express **14**, 8827 (2006).
[38] J. Zhou, T. Koschny, M. Kafesaki, E. N. Economou, J. B. Pendry, and C. M. Soukoulis, Phys. Rev. Lett. **95**, 223902 (2005).

[39] S. Tretyakov, Metamaterials **1**, 40 (2007).
[40] L. D. Landau, E. M. Lifshitz, and L. P. Pitaevskii, *Electrodynamics of Continuous Media* (Elsevier, New York, 2013), Vol. 8.
[41] E. Tatartschuk, N. Gneiding, F. Hesmer, A. Radkovskaya, and E. Shamonina, J. Appl. Phys. **111**, 094904 (2012).
[42] J. A. Dionne, L. A. Sweatlock, H. A. Atwater, and A. Polman, Phys. Rev. B **72**, 075405 (2005).